EXOPLANETS

A Neptune-mass exoplanet in close orbit around a very low-mass star challenges formation models

Guðmundur Stefánsson[1]*, Suvrath Mahadevan[2,3,4], Yamila Miguel[5,6], Paul Robertson[7], Megan Delamer[2,3], Shubham Kanodia[8], Caleb I. Cañas[9], Joshua N. Winn[1], Joe P. Ninan[10], Ryan C. Terrien[11], Rae Holcomb[7], Eric B. Ford[2,3,12,13], Brianna Zawadzki[2,3], Brendan P. Bowler[14], Chad F. Bender[15], William D. Cochran[16,17], Scott Diddams[18,19,20], Michael Endl[16,14], Connor Fredrick[19,20], Samuel Halverson[21], Fred Hearty[2,3], Gary J. Hill[17,14], Andrea S. J. Lin[2,3], Andrew J. Metcalf[22,19,20], Andrew Monson[15], Lawrence Ramsey[2,3], Arpita Roy[23,24]†, Christian Schwab[25], Jason T. Wright[2,3,26], Gregory Zeimann[27,17]

Theories of planet formation predict that low-mass stars should rarely host exoplanets with masses exceeding that of Neptune. We used radial velocity observations to detect a Neptune-mass exoplanet orbiting LHS 3154, a star that is nine times less massive than the Sun. The exoplanet's orbital period is 3.7 days, and its minimum mass is 13.2 Earth masses. We used simulations to show that the high planet-to-star mass ratio ($>3.5 \times 10^{-4}$) is not an expected outcome of either the core accretion or gravitational instability theories of planet formation. In the core-accretion simulations, we show that close-in Neptune-mass planets are only formed if the dust mass of the protoplanetary disk is an order of magnitude greater than typically observed around very low-mass stars.

Low-mass red dwarf stars—those with spectra classified as M dwarfs—are the most common stars close to the Sun and throughout the Milky Way Galaxy (*1*, *2*). Gas giant planets are much rarer around M dwarfs than the more massive F, G, and K dwarf stars (*3*), and the vast majority of planets orbiting M dwarfs are less massive than Neptune (*4*, *5*). Few planets have been detected orbiting the least massive (<0.25 solar masses) and coolest M dwarfs, known as very low-mass dwarfs. This is because very low-mass dwarfs are faint and emit most of their radiation at infrared wavelengths, at which exoplanet detection techniques are less sensitive than at optical wavelengths.

The planetary systems around very low-mass dwarfs TRAPPIST-1 (*6*) and Teegarden's star (*7*) both contain compact systems of small (probably rocky) planets. The formation of such systems is compatible with the core-accretion theory of planet formation (*8*–*11*), within which the outcome depends strongly on the total mass of small solid particles (dust) within the protoplanetary disk from which the planets formed (*9*). Observations of dust disk masses of protoplanetary disks have shown that typical disk dust masses are lower than required to explain observed planetary systems around other stars (*12*, *13*). Protoplanetary disk dust masses are observed to scale with stellar mass (*14*, *15*), implying that the disks around very low-mass stars might have dust masses sufficient to form Earth-mass planets but not giant planets. However, the uncertainties in theoretical models and the large dispersion in observed dust masses are consistent with a small fraction of low-mass stars hosting close-orbiting planets with a mass of $\gtrsim$10 Earth masses ($M_\oplus$).

Massive planet candidates have been detected around a few very low-mass dwarfs, but in all cases, the planets have very wide orbits. Examples include GJ 3512 b [mass, >0.46 Jupiter masses (M_{jup}); orbital period of 203 days] (*16*) and TZ Ari b (mass, >0.21M_{jup}; orbital period of 771 days) (*17*). These gas giants were interpreted as having formed through a mechanism other than core accretion, such as gravitational instability within a massive gaseous outer disk, which produces more wide-orbiting planets than close-orbiting planets (*18*). Giant planets have not been observed on close orbits around very low-mass dwarfs.

A planet orbiting LHS 3154

We observed the low-mass M dwarf LHS 3154 (coordinates are provided in Table 1), located 15.7531 ± 0.0084 pc from the Sun. We used the Habitable-zone Planet Finder (HPF) (*19*, *20*), a near-infrared spectrograph (resolving power R = 55,000) on the 10-m Hobby-Eberly Telescope (HET) at McDonald Observatory in Texas, USA (*21*, *22*). The observations were taken as part of a survey designed to search for planets around very low-mass dwarfs (*19*). We obtained 137 spectra between 23 January 2020 and 13 April 2022, from which we measured the radial velocity (RV) (Fig. 1A) (*23*). A periodogram of the RV data (Fig. 1B) indicates a periodic Doppler shift, which we interpret as being due to a planet with an orbital period of 3.7 days; the corresponding false-alarm probability is $\ll$0.1%. The RV residuals (Fig. 1, B and E) contain no evidence of another planet in the system. The only other peak in the periodogram with <0.1% false alarm probability is a 1-day alias of the 3.7-day period (Fig. 1C).

We fitted a one-planet orbital model to the RV data (*23*). The measured properties of LHS 3154 and our inferred properties of the orbiting planet, LHS 3154 b, are summarized in Table 1. We estimate the stellar mass and radius as 0.1118 ± 0.0027 solar masses ($M_\odot$) and 0.1405 ± 0.0038 solar radii ($R_\odot$), respectively, on the basis of scaling relationships for M dwarfs (*24*, *25*). All uncertainties are 1σ unless stated otherwise. We determined the stellar effective temperature (T_{eff}) as 2861 ± 77 K using the HPF-SpecMatch (*26*) software, which compares a given HPF spectrum with a library of other spectra with known properties. The metallicity of the star (its proportion of elements heavier than helium), which is difficult to constrain for very low-mass stars, is consistent with the Sun's metallicity (*23*). The low eccentricity of LHS 3154b, $e = 0.076^{+0.057}_{-0.047}$, is consistent with a circular orbit at 95% confidence.

Excluding nonplanetary explanations

Stellar activity, the intrinsic variations of a star's atmosphere, can produce apparent radial-

[1]Department of Astrophysical Sciences, Princeton University, Princeton, NJ 08540, USA. [2]Department of Astronomy and Astrophysics, The Pennsylvania State University, University Park, PA 16802, USA. [3]Center for Exoplanets and Habitable Worlds, The Pennsylvania State University, University Park, PA 16802, USA. [4]Institute for Particle Physics and Astrophysics, Eidgenössische Technische Hochschule Zurich, 8092 Zurich, Switzerland. [5]Leiden Observatory, Leiden University, 2300 RA Leiden, Netherlands. [6]Space Research Organisation of the Netherlands, NL-3584 CA Utrecht, Netherlands. [7]Department of Physics and Astronomy, University of California Irvine, Irvine, CA 92697, USA. [8]Earth and Planets Laboratory, Carnegie Institution for Science, Washington, DC 20015, USA. [9]NASA Goddard Space Flight Center, Greenbelt, MD 20771, USA. [10]Department of Astronomy and Astrophysics, Tata Institute of Fundamental Research, Mumbai 400005, India. [11]Department of Physics and Astronomy, Carleton College, Northfield, MN 55057, USA. [12]Center for Astrostatistics, The Pennsylvania State University, University Park, PA 16802, USA. [13]Institute for Computational and Data Sciences, The Pennsylvania State University, University Park, PA 16802, USA. [14]Department of Astronomy, The University of Texas at Austin, Austin, TX 78712, USA. [15]Steward Observatory, University of Arizona, Tucson, AZ 85721, USA. [16]Center for Planetary Systems Habitability, The University of Texas at Austin, Austin, TX 78712, USA. [17]McDonald Observatory, The University of Texas at Austin, Austin, TX 78712, USA. [18]Electrical, Computer and Energy Engineering, University of Colorado, Boulder, CO 80305, USA. [19]National Institute of Standards and Technology, Boulder, CO 80305, USA. [20]Department of Physics, University of Colorado, Boulder, CO 80309, USA. [21]Jet Propulsion Laboratory, California Institute of Technology, Pasadena, CA 91109, USA. [22]Space Vehicles Directorate, Air Force Research Laboratory, Kirtland AFB, NM 87117, USA. [23]Space Telescope Science Institute, Baltimore, MD 21218, USA. [24]Department of Physics and Astronomy, Johns Hopkins University, Baltimore, MD 21218, USA. [25]School of Mathematical and Physical Sciences, Macquarie University, Sydney, NSW 2109, Australia. [26]Penn State Extraterrestrial Intelligence Center, The Pennsylvania State University, University Park, PA 16802, USA. [27]Hobby-Eberly Telescope, University of Texas at Austin, Austin, TX 78712, USA.

*Corresponding author. Email: gstefansson@princeton.edu

†Present address: Schmidt Futures, New York, NY 10011, USA.

velocity shifts that can be misidentified as a planetary signal (*27*). We used several metrics to assess the stellar activity of LHS 3154—including the differential line width indicator and the chromatic index indicators (*7*)—and found no correlation between the RV signal and activity indicators in the HPF spectra (*23*). We obtained an additional optical spectrum of LHS 3154 using the Low-Resolution Spectrograph (LRS2) (*28*) on the HET (resolving power R = 2500), which showed no evidence of emission in the Hα line. Previous work (*29*) has shown that very low-mass M dwarfs without detectable Hα emission rotate slowly; we used their scaling relationship to estimate the rotation period of LHS 3154 as 114 ± 22 days. Such slow rotation is consistent with the narrow stellar lines in the HPF spectra. Time-series photometry from the Transiting Exoplanet Survey Satellite (*30*) shows no evidence of stellar rotation–induced photometric variability at short periods (<10 days), nor of flaring. Time-series photometry over a longer time span from the Zwicky Transient Facility (ZTF) (*31*) shows no evidence for variability on time scales near the 3.7-day period of the planetary signal but does show evidence for variations on time scales between 90 and 140 days (*23*), which is consistent with our estimated rotation rate. We therefore conclude that LHS 3154b is a slowly rotating inactive star and that the 3.7-day RV signal is not caused by stellar activity.

The model fitted to the RVs indicates that LHS 3154b has a minimum mass of $m\sin i = 13.15^{+0.84}_{-0.82}\ M_\oplus$, where m is the planet mass and i is the orbital inclination (which is unknown). To derive an upper limit on the planet's mass, we used astrometric information from the Gaia spacecraft. A sufficiently massive companion would induce detectable astrometric motion, which would appear as excess astrometric noise in the Gaia data (*32*). For LHS 3154, the Gaia Data Release 3 (*33*) catalog reported an excess astrometric noise of 316 micro–arc sec with a significance of 27.7σ. However, the data release does not specify the time scale of the astrometric variability, making it impossible to determine whether it is from the 3.7-day planet or an additional long-period companion. Gaia astrometry for very red stars is known to be affected by larger systematic errors than for Sun-like stars (*34*, *35*), so the significance of the astrometric excess noise is likely overestimated. The Gaia renormalized unit-weight error (RUWE) parameter accounts for the color-dependent systematic issues and has been shown to be a better indicator of a companion object than is the astrometric excess (*34*). LHS 3154's RUWE value of 1.12 (*33*) is consistent with a single star. Even so, if we assume that all of the observed excess astrometric noise is due to a planet on a 3.7-day orbit, and assuming a single-star astrometric solution (*36*), we obtain a 3σ mass limit of $<32M_{\rm jup}$.

Table 1. Properties of the star LHS 3154 and planet LHS 3154b. The stellar parameters were derived by using the HPF-SpecMatch code applied to the HPF spectra (*23*) and scaling relations for M dwarfs (*24*, *25*). The Hα emission is given as the logarithmic ratio of Hα luminosity ($L_{\rm H\alpha}$) to the overall bolometric luminosity ($L_{\rm bol}$). The planet parameters were derived from an orbital model fitted to the HPF RVs (*23*). Median values are listed, and uncertainties denote the 68% credible intervals. Right ascension and declination coordinates are on the International Celestial Reference System (ICRS) at epoch 2016.0. $\rm BJD_{TDB}$ is the barycentric Julian date. The rotation period is estimated from a scaling relationship for inactive M stars (*29*).

Stellar parameters	Value	Reference
Right ascension	$16^h\ 06^m\ 32^s.78$	(*33*)
Declination	+40°54′24″.64	(*33*)
Absolute radial velocity (km s^{-1})	−42.05 ± 0.34	This work
Spectral type	M6.5	This work
V-band magnitude	17.65 ± 0.20	(*45*)
TESS magnitude	13.2266 ± 0.007	(*45*)
J-band magnitude	11.05 ± 0.018	(*45*)
K_S-band magnitude	10.072 ± 0.019	(*45*)
Effective temperature (K)	2861 ± 77	This work
Mass (solar masses, $M_\odot$)	0.1118 ± 0.0027	This work
Radius (solar radii, $R_\odot$)	0.1405 ± 0.0038	This work
Luminosity (solar luminosities, $L_\odot$)	$0.0019^{+0.00015}_{-0.00014}$	This work
Distance (pc)	15.7531 ± 0.0084	(*46*)
Rotation period (days)	114 ± 22	This work
Space velocities (km s^{-1})	U = −42.32 ± 0.10, V = −54.53 ± 0.21, W = 4.16 ± 0.25	This work
Age (10^9 years)	5^{+4}_{-2}	This work
Hα emission ($\log L_{\rm H\alpha}/L_{\rm bol}$)	≤−5.3	This work
Projected rotational velocity (km s^{-1})	<2	This work
Planet parameters		
Orbital period (days)	$3.71778^{+0.00080}_{-0.00081}$	This work
Time of conjunction ($\rm BJD_{TDB}$)	$2458874^{+0.14}_{-0.14}$	This work
Time of periastron ($\rm BJD_{TDB}$)	$2458874.02^{+0.67}_{-0.57}$	This work
Eccentricity	$0.076^{+0.057}_{-0.047}$	This work
Argument of periastron (deg)	82^{+102}_{-47}	This work
Radial velocity semiamplitude (m s^{-1})	$23.4^{+1.5}_{-1.4}$	This work
Minimum mass m sin i ($M_\oplus$)	$13.15^{+0.84}_{-0.82}$	This work
Orbital semimajor axis (au)	0.02262 ± 0.00018	This work

This rules out a stellar binary companion as the origin of the RV variations. Only inclinations ≤0.2° would lead to a mass above $13M_{\rm jup}$, the approximate minimum mass for deuterium fusion, which is sometimes used to distinguish giant planets from brown dwarfs. Although such an orientation would occur in only ~10^{-5} of randomly oriented orbital planes, RV surveys are known to detect such face-on systems and misidentify them as planet candidates (*37*). Given the known low occurrence rate of brown dwarfs on short-period orbits (*38*), and the astrometric constraint of $<32M_{\rm jup}$, we favor the interpretation that LHS 3154 b is a planetary mass object.

Comparison with planet formation models

In Fig. 2, we compare the planet-to-star mass ratio of LHS 3154b with planets around other very low-mass M dwarfs, restricted to those with masses known to within 30%. We used LHS 3154b's mass ratio of 3.5×10^{-4} to test theories of planet formation around low-mass stars.

In the core-accretion model of planet formation, planets grow from initial over densities (known as cores) in a protoplanetary disk, which accrete dust and gas from the surrounding disk. Models in which initial cores grow through the accretion of ~1-km-sized solid bodies (called planetesimals) (*8*–*10*, *39*), or by accreting pebble-sized material (*40*, *41*), predict that very low-mass stars are only capable of forming compact systems of rocky planets on short-period orbits. The maximum mass of planets formed through core accretion in simulations of the planetesimal-driven scenario around low-mass stars is about $5M_\oplus$ (*9*), and $3M_\oplus$ in the pebble accretion–driven scenario (*40*, *41*). With a

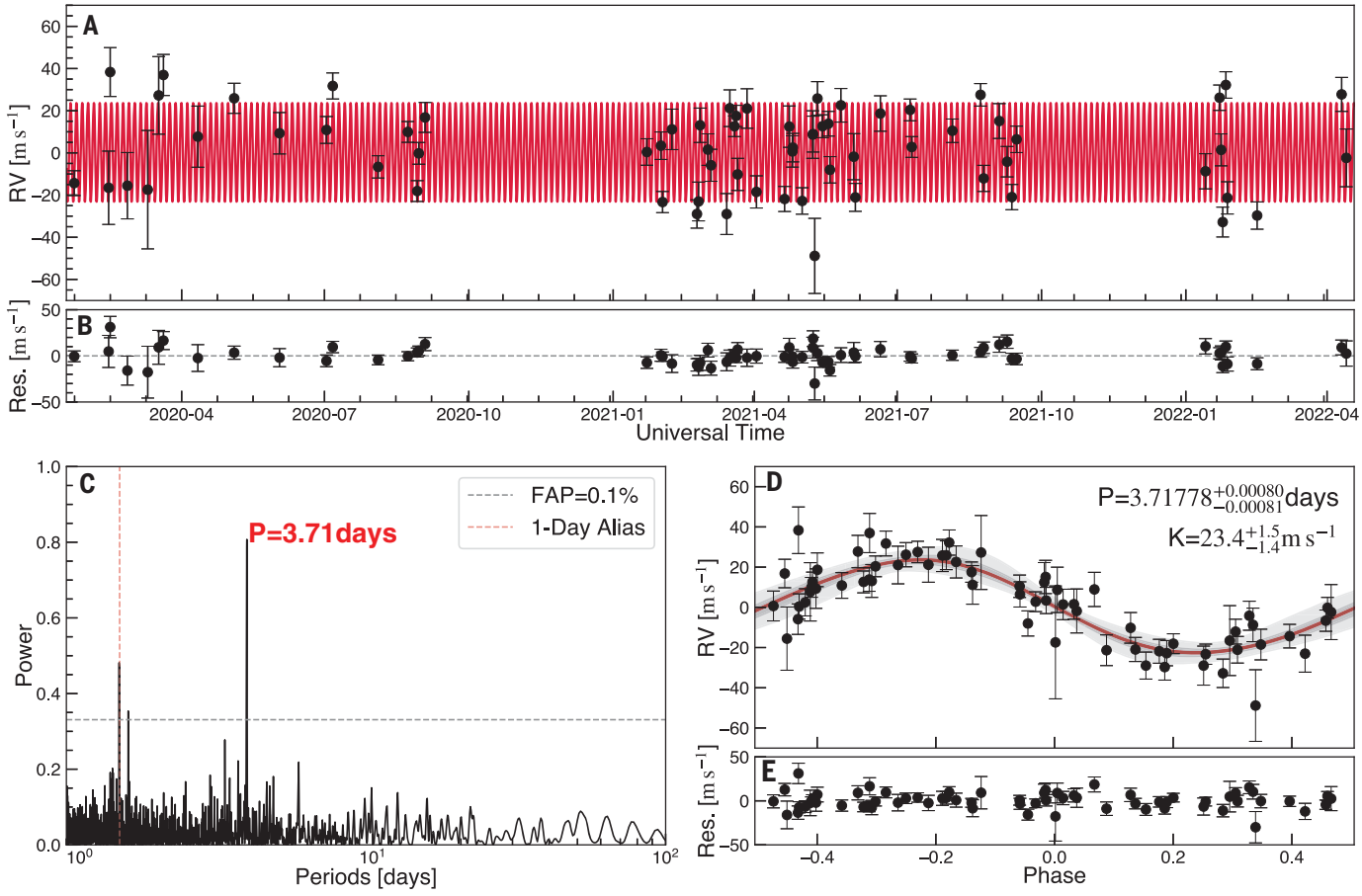

Fig. 1. HPF radial velocity observations of LHS 3154b. (**A**) Radial velocity (RV) as a function of Universal Time date (black data points) and the orbital model fitted to the data (red line). The parameters of the model are listed in Table 1. (**B**) Residuals (black data points) between the RV observations and the model. The gray dashed line indicates 0 m s^{-1}. (**C**) Periodogram of the RV data (black; arbitrary units). A peak at 3.7 days is labeled in red. The vertical red dashed line indicates the 1-day alias of the 3.7 peak. The black horizontal dashed line indicates the 0.1% false-alarm probability (FAP) line. (**D**) Phase-folded radial velocities. The best-fitting period *P* and RV semiamplitude *K* are listed at top right and in Table 1. The red curve is the best-fitting model, and the grey shading indicates the 1σ and 3σ credible regions, respectively. (**E**) Phase-folded residuals. All error bars denote 1σ uncertainties.

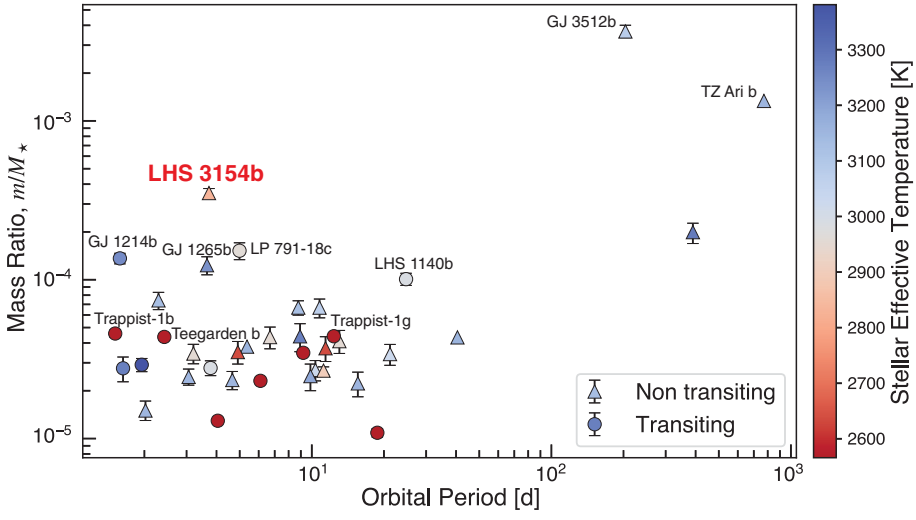

Fig. 2. Planet-to-star mass ratios for planets orbiting very low-mass stars. The sample is restricted to planet mass measurements (*m*) with an uncertainty smaller than 30% and host star masses of $M_\star < 0.25M_\odot$. Circles indicate transiting planets with measured masses. Triangles indicate planets detected with the RV technique, for which only a lower mass limit (*m* sin *i*) is available. Colors indicate the host star stellar effective temperature (color bar). LHS 3154b is in red; black labels indicate other exoplanets discussed in the text and other M dwarf planets with high planet-to-star mass ratios. Error bars denote 1σ uncertainties and are shown for all planets; in some cases, they are smaller than the symbol size.

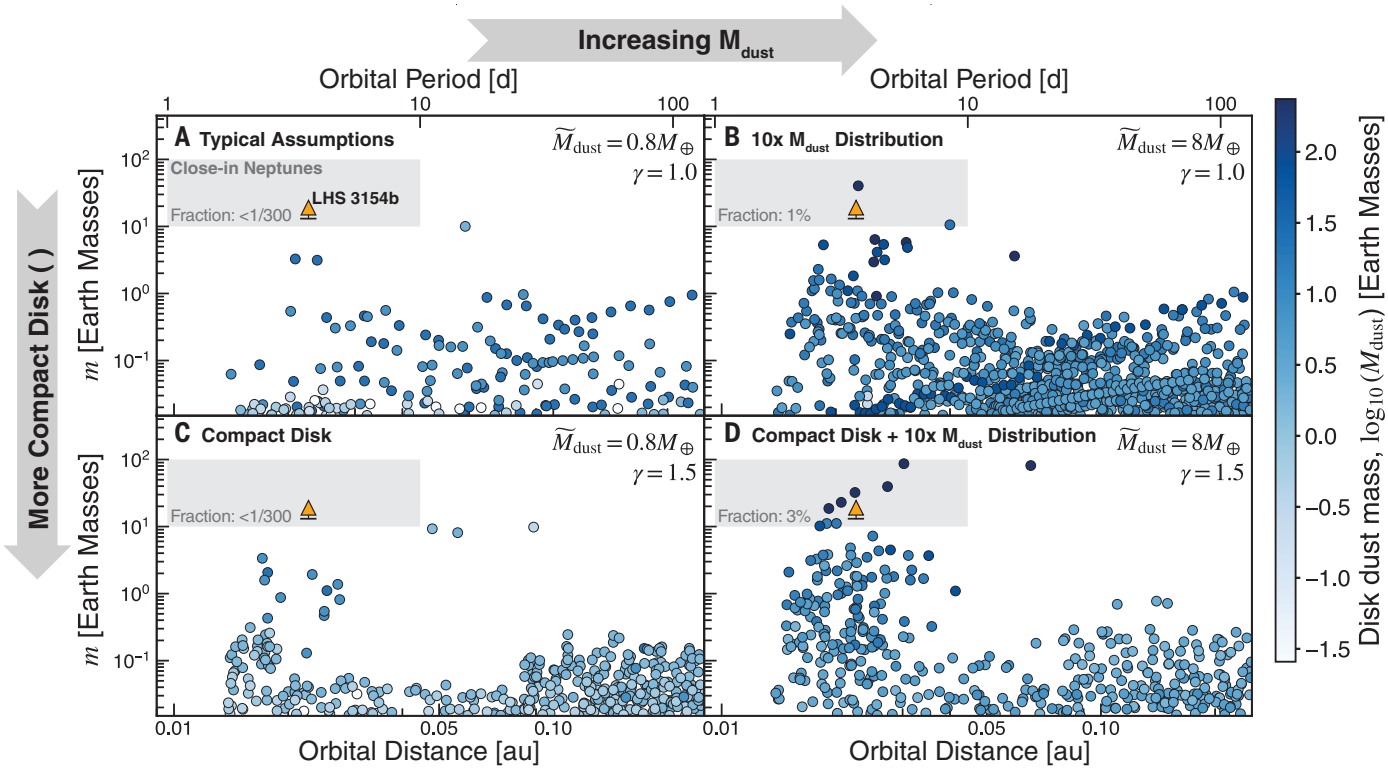

Fig. 3. Results from our simulations of core-accretion planet formation. Planet mass is shown as a function of orbital distance in astronomical units (au). Circles indicate results from simulated systems, 300 in each panel, colored by the disk dust mass in that simulation. LHS 3154b is indicated with an orange arrow in (A) to (D), with its base indicating the minimum mass of 13.2 Earth masses. Gray boxes highlight the region and corresponding frequencies of close-in Neptune-mass planets (periods from 1 to 10 days and masses from 10 to 100 Earth masses) formed in the simulations. (**A**) Results from typical assumptions (*23*), drawing the protoplanetary disk dust mass M_{dust} from a distribution with a median of $\tilde{M}_{dust} = 0.8M_{\oplus}$ and a disk power law index of $\gamma = 1.0$. (**B**) Same as in (A) but with higher median of the disk dust mass distribution, by an order of magnitude, with $\tilde{M}_{dust} = 8M_{\oplus}$. (**C**) Same as in (A) but with $\gamma = 1.5$. (**D**) Same as in (B) but with $\gamma = 1.5$. Typical assumptions of planet formation (A) are incapable of forming planets as massive as LHS 3154b around $0.1M_{\odot}$ stars. To form LHS 3154b–mass planets requires us to increase the mass of the disk (B), preferably in more compact disks (D) that have higher dust surface densities close to the star, facilitating formation of close-in massive planets.

minimum mass of $13.2M_{\oplus}$, LHS 3154b is difficult to explain with core-accretion models.

Core-accretion simulations

The outcomes of planet-formation models depend sensitively on the assumed protoplanetary disk properties, especially the total disk dust mass and its surface-density distribution as a function of distance from the star. We performed planet-formation simulations for the LHS 3154 system based on the core-accretion scenario by modifying a previous model (*9*) to include gas accretion (supplementary text) (*23*, *42*).

We show in Fig. 3 the resulting simulation outcomes for four combinations of assumed total disk mass and disk surface density distribution, the latter parameterized by a power law index γ. Results are shown in Fig. 3A from simulations in which the disk dust masses are drawn from a distribution of masses consistent with observations for a $0.1M_{\odot}$ star (*15*) and a nominal surface density distribution with power law index $\gamma = 1$ (*23*). Simulations with these parameters do not form any close-orbiting planets as massive as LHS 3154b. The results from simulations in which the median mass of the disk dust mass distribution has been increased by an order of magnitude are shown in Fig. 3B. Simulation results are shown in Fig. 3, C and D, for the same mass distributions as in Fig. 3, A and B, but in more compact disks ($\gamma = 1.5$). A small number of planets with properties similar to those of LHS 3154b are produced in the two simulations with higher total dust mass distributions (Fig. 3, B and D). In those simulations, the larger amounts of solid material produce on average more massive initial cores, which can grow into more massive planets. The more compact disks increase the density of dust close to the star, leading to more collisions that form close orbiting planets. However, we found that more compact disks alone, without larger dust disk masses (Fig. 3C), do not form planets similar to LHS 3154b in our simulations.

Gravitational instability models

Another possible way to form massive planets is through gravitational instability, which has been invoked to explain massive gas giant planets around low-mass stars, such as the wide-orbiting gas giant planet GJ 3512b (mass $>0.46M_{jup}$; P = 203 days) (*16*). However, LHS 3154b's mass of $13.2M_{\oplus}$ is much lower than the minimum mass of planets formed from gravitational instability: Simulations of gravitational instability around a $0.1M_{\odot}$ star found minimum mass fragments of $\sim 60M_{\oplus}$ (*16*)—about five times larger than the lower limit for LHS 3154b. Gravitational instability preferentially forms planets on wide orbits (*16*). Although we cannot rule out the gravitational instability mechanism, if LHS 3154b formed through gravitational instability followed by inward migration, it would require even greater protoplanetary disk masses than we considered above for the core-accretion scenario.

High disk masses

Both potential formation mechanisms require protoplanetary disks that have substantially greater dust masses than are typically observed around very low-mass stars (*15*). One possible solution to this discrepancy is if a large fraction of the dust in protoplanetary disks around

low-mass stars grows to centimeter sizes or more (*43*, *44*); pebbles of that size would not be detected by the millimeter observations used to estimate the overall dust masses, causing them to underestimate. Another possibility is that disks accrete large amounts of additional material from the surrounding parent molecular cloud (*12*). A third possibility is that protoplanetary cores form soon (within 1 million years) after the host protostar, when protoplanetary disks are expected to be more massive than at later times. This would enable runaway accretion of gases and thereby the formation of a gas giant planet (*13*).

REFERENCES AND NOTES

1. T. J. Henry *et al*., *Astron. J.* **132**, 2360–2371 (2006).
2. J. G. Winters *et al*., *Astron. J.* **149**, 5 (2015).
3. M. Endl *et al*., *Astrophys. J.* **649**, 436–443 (2006).
4. X. Bonfils *et al*., *Astron. Astrophys.* **549**, A109 (2013).
5. S. Sabotta *et al*., *Astron. Astrophys.* **653**, A114 (2021).
6. M. Gillon *et al*., *Nature* **542**, 456–460 (2017).
7. M. Zechmeister *et al*., *Astron. Astrophys.* **627**, A49 (2019).
8. Y. Alibert, W. Benz, *Astron. Astrophys.* **598**, L5 (2017).
9. Y. Miguel, A. Cridland, C. W. Ormel, J. J. Fortney, S. Ida, *Mon. Not. R. Astron. Soc.* **491**, 1998 (2020).
10. B. Zawadzki, D. Carrera, E. B. Ford, *Mon. Not. R. Astron. Soc.* **503**, 1390–1406 (2021).
11. R. Burn *et al*., *Astron. Astrophys.* **656**, A72 (2021).
12. C. F. Manara, A. Morbidelli, T. Guillot, *Astron. Astrophys.* **618**, L3 (2018).
13. S. M. Andrews, *Annu. Rev. Astron. Astrophys.* **58**, 483–528 (2020).
14. M. Ansdell *et al*., *Astrophys. J.* **828**, 46 (2016).
15. I. Pascucci *et al*., *Astrophys. J.* **831**, 125 (2016).
16. J. C. Morales *et al*., *Science* **365**, 1441–1445 (2019).
17. A. Quirrenbach *et al*., *Astron. Astrophys.* **663**, A48 (2022).
18. A. Mercer, D. Stamatellos, *Astron. Astrophys.* **633**, A116 (2020).
19. S. Mahadevan *et al*., *Proc. SPIE* **8446**, 84461S (2012).
20. S. Mahadevan *et al*., *Proc. SPIE* **9147**, 91471G (2014).
21. L. W. Ramsey *et al*., *Proc. SPIE* **3352**, 34–42 (1998).
22. G. J. Hill *et al*., *Astron. J.* **162**, 298 (2021).
23. Materials and methods are available as supplementary matrials.
24. A. W. Mann, G. A. Feiden, E. Gaidos, T. Boyajian, K. von Braun, *Astrophys. J.* **804**, 64 (2015).
25. A. W. Mann *et al*., *Astrophys. J.* **871**, 63 (2019).
26. G. Stefansson *et al*., *Astron. J.* **159**, 100 (2020).
27. P. Robertson, S. Mahadevan, M. Endl, A. Roy, *Science* **345**, 440–444 (2014).
28. T. S. Chonis *et al*., *Proc. SPIE* **9908**, 99084C (2016).
29. E. R. Newton *et al*., *Astrophys. J.* **834**, 85 (2017).
30. G. R. Ricker *et al*., *J. Astron. Telesc. Instrum. Syst.* **1**, 014003 (2015).
31. F. J. Masci *et al*., *Publ. Astron. Soc. Pac.* **131**, 018003 (2019).
32. P. Kervella, F. Arenou, F. Mignard, F. Thévenin, *Astron. Astrophys.* **623**, A72 (2019).
33. Gaia Collaboration *et al*., *Astron. Astrophys.* **674**, A34 (2023).
34. C. Ziegler *et al*., *Astron. J.* **156**, 259 (2018).
35. P. C. Thao *et al*., *Astron. J.* **159**, 32 (2020).
36. Z. Penoyre, V. Belokurov, N. Wyn Evans, A. Everall, S. E. Koposov, *Mon. Not. R. Astron. Soc.* **495**, 321–337 (2020).
37. J. T. Wright *et al*., *Astrophys. J.* **770**, 119 (2013).
38. B. Ma, J. Ge, *Mon. Not. R. Astron. Soc.* **439**, 2781–2789 (2014).
39. M. Pan, S. Wang, J. Ji, *Mon. Not. R. Astron. Soc.* **510**, 4134–4145 (2022).
40. B. Liu, M. Lambrechts, A. Johansen, I. Pascucci, T. Henning, *Astron. Astrophys.* **638**, A88 (2020).
41. S. Dash, Y. Miguel, *Mon. Not. R. Astron. Soc.* **499**, 3510–3521 (2020).
42. S. Ida, D. N. C. Lin, *Astrophys. J.* **616**, 567–572 (2004).
43. J. P. Williams, *Meteorit. Planet. Sci.* **47**, 1915–1921 (2012).
44. Y. Liu *et al*., *Astron. Astrophys.* **668**, A175 (2022).
45. K. G. Stassun *et al*., *Astron. J.* **158**, 138 (2019).
46. C. A. L. Bailer-Jones, J. Rybizki, M. Fouesneau, M. Demleitner, R. Andrae, *Astron. J.* **161**, 147 (2021).
47. G. Stefansson, HPF-SERVAL release, v. 1.0.0. Zenodo (2023); https://doi.org/10.5281/zenodo.8397170.
48. G. Stefansson *et al*., Planet Formation Simulations For LHS 3154, v.1.0.0. Zenodo (2023); https://doi.org/10.5281/zenodo.8402572.

ACKNOWLEDGMENTS

We thank the three anonymous referees for their helpful comments and suggestions, which improved the quality of this paper. Computations were performed at the Pennsylvania State University's Institute for Computational and Data Sciences (ICDS). The Hobby-Eberly Telescope (HET) is a joint project of the University of Texas at Austin, the Pennsylvania State University, Ludwig-Maximilians-Universität München, and Georg-August-Universität Göttingen. The HET is named in honor of its principal benefactors, William P. Hobby and Robert E. Eberly. The Low Resolution Spectrograph 2 (LRS2) was developed and funded by the University of Texas at Austin McDonald Observatory and Department of Astronomy and by Pennsylvania State University. We thank the Leibniz-Institut für Astrophysik Potsdam (AIP) and the Institut für Astrophysik Göttingen (IAG) for their contributions to the construction of the integral field units. **Funding:** This work was partially supported by funding from the Center for Exoplanets and Habitable Worlds, which is supported by the Pennsylvania State University, the Eberly College of Science, and the Pennsylvania Space Grant Consortium. G.S. acknowledges support provided by NASA through the NASA Hubble Fellowship grant HST-HF2-51519.001-A awarded by the Space Telescope Science Institute, which is operated by the Association of Universities for Research in Astronomy, for NASA under contract NAS5-26555. Y.M. acknowledges support from the European Research Council (ERC) under the European Union's Horizon 2020 research and innovation program (grant agreement 101088557, N-GINE). C.I.C. acknowledges support through an appointment to the NASA Postdoctoral Program at the Goddard Space Flight Center administered by Oak Ridge Associated Universities through a contract with NASA. We acknowledge support from NSF grants AST-1006676 (S.M., C.F.B., and L.R), AST-1126413 (S.M., C.F.B., L.R., R.C.T., A.R., G.S., and P.R.), AST-1310885 (S.M. and C.F.B), AST-1310875 (S.D, A.J.M, and C.F.), AST-2108493 (P.R.), AST-2108512 (S.M. and M.D.), AST-2108569 (R.C.T.), AST-2108801 (W.D.C. and M.E.), the NASA Astrobiology Institute (NAI; NNA09DA76A) (S.M.), and PSARC (S.M.). We acknowledge support from the Heising-Simons Foundation through grant 2017-0494 (M.E.) and 2019-1177 (E.B.F.). S.H. acknowledges support for work performed at the Jet Propulsion Laboratory, California Institute of Technology, which was under a contract with NASA (80NM0018D0004). S.M., P.R., and G.S. performed work as part of NASA's CHAMPs team, supported by NASA under grant 80NSSC23K1399 issued through the Interdisciplinary Consortia for Astrobiology Research (ICAR) program. **Author contributions:** G.S. analyzed the RVs and host star properties, interpreted the results, and led the manuscript writing. S.M. is principal investigator of the HPF instrument, provided oversight, and assisted with analysis and interpretation. Y.M. led the planet-formation simulations, with G.S. providing assistance. P.R. provided leadership in obtaining the HPF observations and worked with G.S. and S.M. on the interpretation of the result. M.D. contributed to the RV analysis and revision of the manuscript. C.I.C. and B.P.B. provided the Gaia upper mass limit constraints and investigated the false-positive scenarios. J.N.W. provided interpretation and revision of the manuscript. G.Z., S.K., G.J.H., and G.S. reduced and interpreted the LRS2 spectra. B.Z. and E.B.F. contributed to the interpretation of the planet formation simulations. R.H. aided with the TESS photometric analysis. J.P.N., C.F.B., A.R., and R.C.T. extracted the HPF spectra and performed wavelength calibration, working with S.D., A.J.M., and C.F. to determine the wavelength solution for the HPF spectra. W.D.C. and M.E. led HPF observing programs used to discover the planet. G.S., S.M., P.R., J.P.N., C.F.B., R.C.T., A.R., S.H., S.K., F.H., A.S.J.L., A.M., L.R., C.S., and J.T.W. contributed to the design, monitoring, and execution of the HPF Survey, during which these observations were carried out. All authors contributed to the interpretation of the result. **Competing interests:** The authors declare no competing interests. **Data and materials availability:** The HPF radial velocities and activity indicators are provided as machine-readable files in data S1 and data S2, respectively. The 137 HPF spectra are available on Zenodo (*47*). The HPF-SERVAL code used to extract the RVs is available at https://github.com/gummiks/hpfserval_lhs3154 and is archived in the same Zenodo repository (*47*). The planet formation simulation code is available at https://github.com/AstroYamila-Team/PlanetFormation_SmallStars and is also archived on Zenodo (*48*).

SUPPLEMENTARY MATERIALS

science.org/doi/10.1126/science.abo0233
Materials and Methods
Supplementary Text
Figs. S1 to S8
Table S1
References (*49*–*91*)
Data S1 and S2

Submitted 17 October 2022; accepted 9 October 2023
10.1126/science.abo0233